Journal of Applied Polymer Science

Preparation of poly(methyl methacrylate-*co*-butyl methacrylate) nanoparticles and their reinforcing effect on natural rubber

Jin Liu, Xiaohui Tian, Jinyu Sun, Yizhong Yuan
School of Materials Science and Engineering, East China University of Science and Technology, Shanghai 200237, China
Correspondence to: X. Tian (E-mail: tianxh@263.net)

ABSTRACT: Poly(methyl methacrylate-*co*-butyl methacrylate) [P(MMA-*co*-BMA)] nanoparticles were synthesized via emulsion polymerization, and incorporated into natural rubber (NR) by latex compounding. Monodispersed, core-shell P(MMA-*co*-BMA)/casein nanoparticles (abbreviated as PMBMA-CA) were produced with casein (CA) as surfactant. The chemical structure of P(MMA-*co*-BMA) copolymers were confirmed by ^{1}H-NMR and FTIR analyses. Transmission electron microscopy demonstrated the core–shell structure of PMBMA-CA, and PMBMA-CA homogenously distributed around NR particles, indicating the interaction between PMBMA-CA and NR. As a result, the tensile strength and modulus of NR/PMBMA-CA films were significantly enhanced. The tensile strength was increased by 100% with 10% copolymer addition, when the molar ratio of MMA:BMA was 8:2. In addition, scanning electron microscopy and atomic force microscopy results presented that the NR/PMBMA-CA films exhibited smooth surfaces with low roughness, and PMBMA-CA was compatible with NR. FTIR-ATR analyses also suggested fewer PMBMA-CA nanoparticles migrated out of NR. © 2016 Wiley Periodicals, Inc. J. Appl. Polym. Sci. **2016**, *133*, 43843.

KEYWORDS: composites; mechanical properties; morphology; rubber

Received 22 December 2015; accepted 24 April 2016
DOI: 10.1002/app.43843

INTRODUCTION

Natural rubber (NR) latex obtained from *Heva brasiliensis* is an important source of NR products due to its excellent physical properties. NR is widely used in various areas such as adhesives, tyres, surgical gloves, health equipment and accessories, condoms, coating, and floor covering products.[1] NR particles consist of *cis*-polyisoprene core and non-rubber component shell including phospholipids and proteins.[2,3] The non-rubber shell plays an important role in stabilizing the latex particles and also contributing to the outstanding performance of NR.[4] Nevertheless, the tensile strength and modulus of unmodified NR is insufficient to meet the requirements of some products. In order to extend its application, various approaches have been developed to improve the physical properties of NR-based materials.

Polymer blending has gained much attention, since blending two materials usually generates a new product, whose properties are quite different from the individual components.[5] For example, the modulus and hardness of NR have been improved by blending NR with polymers,[6,7] such as poly(vinyl acetate),[8] polystyrene,[9,10] and poly(ethylene glycol).[11] Recently, NR/poly(methyl methacrylate) (PMMA) blends have attracted much attention because PMMA possesses excellent mechanical properties, clarity, and weather resistance.[7] However, the physical properties of NR/PMMA blends have been found to be inferior due to the marked incompatibility of the components.[12,13] Therefore, the technological compatibilization of the immiscible component is strongly required. Oommen *et al.* demonstrated that the copolymer NR-*g*-PMMA, as a compatibilizer, could enhance the interfacial adhesion between NR and PMMA, and consequently strengthen the mechanical properties of the blending polymer.[14,15] It was also reported that the interaction of epoxidized or maleated NR with PMMA could improve the compatibility of the two phases.[16,17] Similarly, interpenetrating polymer networks (IPN) was prepared via polymerizing MMA in NR matrix, which resulted in uniform films with improved phase adhesion and compatibility.[7,18] All these methods are based on the chemical modification of NR, which has been regarded as a preferred way to improve compatibility between NR and PMMA in the past few years.

Increasing physical interaction of NR and PMMA by copolymerizing MMA with relatively flexible monomer provides a convenient approach to resolve the immiscible issue. Copolymerizing MMA with relative flexible butyl methacrylate (BMA) monomer make the copolymer P(MMA-*co*-BMA) easily

Additional Supporting Information may be found in the online version of this article.

penetrate into NR matrix and strengthen interfacial adhesion of NR and the copolymer. Casein (CA), a milk protein, has been applied as emulsifier to prepare well-defined core–shell PMMA/CA nanoparticles.[19,20] Notably, CA could promote emulsion polymerization of MMA, and maintain particle stability.[21] It is also a commonly used stabilizer and dispersant in NR products, which could improve mechanical properties and chemical stability of NR.[22,23] In this study, the poly(methyl methacrylate-*co*-butyl methacrylate) [P(MMA-*co*-BMA)] nanoparticles was synthesized via emulsion polymerization using traditional emulsifier or CA. P(MMA-*co*-BMA) nanoparticles prepared with traditional emulsifier or CA are abbreviated as PMBMA and PMBMA-CA, respectively. The amine groups of CA react with alkyl hydroperoxides, thereby generating macroradicals, which initiate graft copolymerization of vinyl monomers.[24] Then the monodispersed core–shell nanoparticles can be formed by assembling of grafted CA and P(MMA-*co*-BMA) copolymers. The carbonyl and amino groups in CA could interact with the proteins of NR outer layer, then further improving the compatibility between PMBMA-CA and NR. Because of the multi-interactions of BMA and CA with NR, it was found that the PMBMA-CA could be compatible with NR, and resulting in enhanced mechanical properties of NR composites.

EXPERIMENTAL

Materials

High ammonia NR latex (60% dry rubber content) was purchased from Hainan American International Xianghe Industry (Hainan, China). The monomers, methyl methacrylate (MMA, 99%, Aladdin Industrial Inc., Shanghai, China) and BMA (98%, Aladdin Industrial Inc., Shanghai, China), were purified to remove the hydroquinone inhibitor before use. Azobisisobutyronitrile (AIBN, 98%, Aladdin Industrial Inc., Shanghai, China) was recrystallized. *tert*-Butyl hydroperoxide solution (TBHP, 65% aqueous solution, Sinopharm Chemical Reagent. Co., Ltd, Shanghai, China), tween 80, polyvinyl pyrrolidine (PVP, M_w 8000, Aladdin Industrial Inc., Shanghai, China), anhydrous sodium carbonate (Tianjin Zhiyuan Reagent Co. Ltd, Tianjin, China), and sodium dodecyl benzene sulfate (SDBS, Aladdin Industrial Inc. Shanghai, China) were used as purchased. CA (Aladdin Industrial Inc., Shanghai, China) was purified by mixing it with 1% ethylene diamine tetra acetic acid disodium salt (EDTA, Shanghai lingfeng chemical reagent Co., Ltd., Shanghai, China) solution to remove metal ions in the CA. Methanol, methylene chloride, isopropanol, chloroform, and tetrahydrofuran (THF) were obtained from Sigma Aldrich (St. Louis, US) and used without further purification. D-chloroform ($CDCl_3$) for ^{1}H-NMR analysis was obtained from Merck (Darmstadt, Germany). The distilled water was used in all the work.

Synthesis of PMBMA

The emulsion polymerization was performed in a 100 mL flask equipped with nitrogen inlet tube, reflux condenser and dropping funnel. A certain amount of BMA monomer, SDBS (0.5 g), tween 80 (0.5 g) as surfactants, and PVP (0.1g) as dispersing agent were dissolved in 22 mL distilled water. The system was purged with nitrogen for 30 min to remove oxygen and then heated up to 80 °C. After that, the initiator AIBN (0.01 g), dissolved in the monomer MMA, was added to the reaction system at a moderate flow rate. The reaction was kept constant at 80 °C for 8 h, and the obtained emulsion solution was stored in the fridge after sealing. The amount of MMA and BMA was constantly 10.0 g; the ratio of MMA:BMA was 8:2 or 5:5 by molar. The copolymer was precipitated in excess methanol, and the obtained product was dissolved in THF and then repeatedly precipitated in methanol for several times.

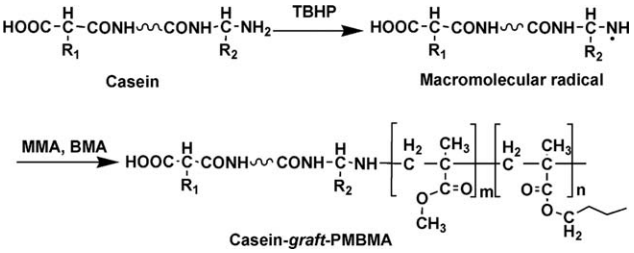

Scheme 1. Synthesis route for CA-*graft*-PMBMA

Synthesis of PMBMA-CA

CA (1.0 g) and anhydrous Na_2CO_3 (0.3 g) were dissolved in 40 mL water; the mixture was stirred at 50 °C under nitrogen for 30 min to completely dissolve the CA. The monomers (5.0 g of MMA and BMA, the molar ratio of MMA:BMA varied from 10:0 to 5:5) were added in the mixed solution, stirred and then purged with nitrogen. After 30 min, TBHP (0.005 g) was added, and the mixture was heated at 80 °C for 8 h under nitrogen. The P(MMA-*co*-BMA) copolymer and CA-*graft*-PMBMA were separeted by Soxhlet extraction using chloroform. The graft copolymerization of MMA, BMA, and CA are presented in Scheme 1.

All the above precipitated P(MMA-*co*-BMA) copolymers were also washed with methylene chloride and then isopropanol to remove PMMA and PBMA homopolymers eventually produced in the copolymerization reactions.[25] After purification, the solid products were dried at 60 °C under vacuum for 12 h. The dried samples were characterized by Fourier transform infrared (FTIR), ^{1}H-NMR, gel permeation chromatography (GPC), and differential scanning calorimetry (DSC) analysis.

Preparation of NR/P(MMA-*co*-BMA) Nanocomposites

A designed amount of PMBMA and PMBMA-CA latices were incorporated into the NR via latex compounding. The pH of the PMBMA and PMBMA-CA latices was adjusted to 10 by adding ammonia solution before use. The mixtures of NR and copolymer latices were stirred in appropriate velocity for 2 h and then stayed overnight. The PMMA and NR blend films were also prepared for comparison. All the procedures were carried out at room temperature. The resultant mixture was poured into polystyrene plates and dried at 70 °C for 6 h.

Characterization Techniques

Nuclear Magnetic Resonance Analysis. The nuclear magnetic resonance (^{1}H-NMR) spectra were obtained using Bruker AVANCEIII NMR spectrometer operated at room temperature using $CDCl_3$ as solvent and TMS as the internal standard.

Fourier Transform Infrared Spectroscopy. Fourier transform infrared (FTIR) analysis was carried out by Magna-IR 550

(Nicolet) instrument. For P(MMA-*co*-BMA) and CA-*graft*-PMBMA copolymers, the purified samples were ground with KBr and then pressed into transparent pellet. ATR accessory was used to obtain FTIR-ATR spectra of NR blend films. The spectra were recorded from 4000 to 400 cm^{-1} at a resolution of 4 cm^{-1} over 20 scans.

Particles Size Analysis. The particle size of each samples were determined with a Berkman coulter delsa Nano C particle analyzer (DLS) at 25 °C at appropriate concentration.

Measurement of Molecular Weight. The molecular weight and polydispersity index (PDI) of the P(MMA-*co*-BMA) copolymers were determined using a Waters 1515 gel permeation chromatograph (GPC) equipped with a refractive index detector and ultrastyragel columns of 100–10,000 Å porosities. The GPC system was calibrated with polystyrene as the standards and THF as the eluent at a flow rate of 1 mL min^{-1}.

Differential Scanning Calorimetry Analysis. DSC was used to characterize the endothermic transition of the substances, and also to confirm the compatibility of each ingredient.[26] The samples (10 mg) was placed in the hermetically sealed aluminum pan and run in the DSC instrument (DSC Q2000, TA, US) from −100 °C to 120 °C at a heating rate of 10 °C min^{-1} under a liquid nitrogen atmosphere.

Transmission Electron Microscope. Internal structural investigation of PMBMA and PMBMA-CA nanoparticles and modified NR latices were investigated with transmission electron microscope (TEM; JEM-1400, JEOL, Japan) working at 120 kV. The diluted solution was dropped onto a copper grid covered with a conductive polymer.

Measurements of Mechanical Properties. Tensile strength, modulus, and elongation at break were determined using a universal testing machine (CMT2203) at 400 mm min^{-1} crosshead speed at room temperature in accordance to test method GB 7543-2006. The dumbbell-shaped specimens with a gauge width of 4 mm were obtained using a punch. The hardness of neat and modified NR films were measured by using a shore A scale hardness tester according to ASTM D2240.

Scanning Electron Microscope. The surface and cross-section morphology of P(MMA-*co*-BMA) modified NR films were examined by scanning electron microscope (SEM; S-4800, Hitachi, Tokyo, Japan). The samples were fractured in liquid nitrogen to obtain the cross-section. Before photographing, all the samples were coated with a conductive layer of sputtered gold.

Atomic Force Microscope. The 3-D images of neat and modified NR films surface were obtained by a NanoScope IIIa multimode atomic microscope (AFM, Veeco, US) at room temperature using tapping mode probes with constant amplitude (200 mV). The surface mean roughness (R_a) was calculated by Nanoscope software.

RESULTS AND DISCUSSION

Characterization of P(MMA-*co*-BMA) Copolymers

The ^{1}H-NMR spectrum of the copolymer (Figure 1) showed a peak at 3.6 ppm, which corresponded to the methoxyl of methyl methacrylate. Similarly, the characteristic peak at 4.0 ppm

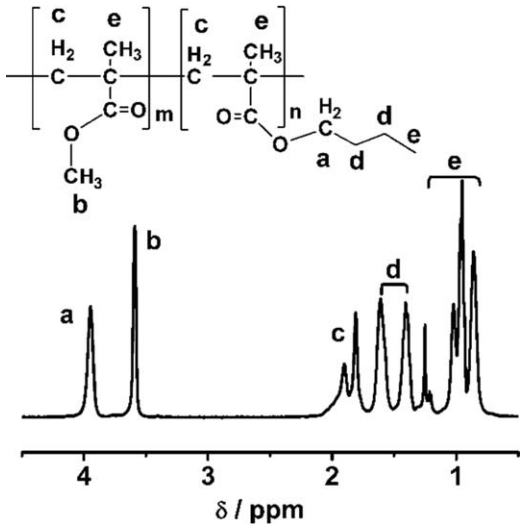

Figure 1. ^{1}H-NMR spectrum of P(MMA-*co*-BMA) copolymer from PMBMA-CA in $CDCl_3$.

attributed to the ethyleneoxy of BMA.[27] These two peaks were identified in all copolymers, confirming the successful copolymerization of the MMA and BMA. The respective monomer compositions of the copolymers were determined from the integrated areas of peak a and peak b. The calculated molar compositions of MMA and BMA for all the P(MMA-*co*-BMA) copolymers are illustrated in Table I. Besides these two characteristic peaks of MMA and BMA, the two peaks at 1.8–1.9 ppm were assigned as the protons of methylene in the main chain. The peaks at 1.6 and 1.4 ppm were attributed to the protons of methylene groups in butyl chain. The peaks at 0.8–1.3 ppm corresponded to the protons of methyl groups in the molecular chain.

Figure 2 presents the FTIR spectra of PMMA, P(MMA-*co*-BMA) copolymer, and PBMA. The spectra of PMMA [Figure 2(a)] illustrated characteristic peaks of C—H asymmetrical stretching vibration for CH_3 at 2994 cm^{-1}, C—H symmetrical stretching vibration for CH_2 at 2844 cm^{-1}, C═O stretching vibration at 1730 cm^{-1}, C—H in-plane bending vibration for CH_3 at 1445 cm^{-1} and C—O stretching vibration at 1153 cm^{-1}. After the copolymerization, the spectrum of the P(MMA-*co*-BMA) copolymer [Figure 2(b)] revealed some new signals corresponding to PBMA segment [Figure 2(c)]. As shown in Figure 2(b), the new peaks at 2930, 2875, and 1463 cm^{-1} corresponded to the C—H stretching of CH_3 adjacent to —$CH_2CH_2CH_2$—, C—H symmetrical stretching, and C—H scissoring vibration of CH_2 in the aliphatic chain.[28] These results further confirmed the successful copolymerization of MMA and BMA. In addition, the FTIR spectrum of the CA-*graft*-PMBMA (Supporting Information Figure S1) separated from PMBMA-CA showed peaks at 1730 cm^{-1}, 1460 cm^{-1}, and 1410 cm^{-1}, indicating the P(MMA-*co*-BMA) copolymer grafted onto CA. The spectrum of CA presented double peaks at 3302 cm^{-1} and 3408 cm^{-1} [Supporting Information Figure S1(a1)], which belonged to asymmetric and symmetric N—H stretching of –NH_2.[29] However, the spectrum of CA-*graft*-PMBMA only had a single peak at 3420 cm^{-1} [Supporting Information Figure S1(a2)],

Table I. Particle Size, Molar Composition, GPC, and DCS Analyses of P(MMA-*co*-BMA) Nanoparticles

Samples	Mean diameter (nm)	PDI[a]	M_n[b] (Da)	M_w[b] (Da)	DI (M_n/M_w)	Molar composition[c] MMA:BMA	T_g[d] (°C)
PMBMA1[e]	83.5	0.213	367,000	720,000	1.96	8.1:1.9	88
PMBMA2[f]	82.0	0.238	413,000	807,000	1.95	5.2:4.8	56
PMBMA-CA1[e]	158.6	0.093	313,000	603,000	1.93	7.9:2.1	90
PMBMA-CA2[f]	166.5	0.080	369,000	632,000	1.71	4.9:5.1	52

[a] PDI, polydispersity index.
[b] The M_n and M_w were obtained from GPC analysis.
[c] The molar composition was calculated from ^{1}H-NMR spectra.
[d] T_g values were evaluated by DSC.
[e] Feeding ratio of MMA:BMA is 8:2 by mole.
[f] Feeding ratio of MMA:BMA is 5:5 by mole.

which means the primary amine (—NH_2) changed into secondary amine (—NH—) after graft copolymerization. And the peaks at 1652 cm^{-1} and 1538 cm^{-1}, assigning to —C═O stretching and —NH— bending of CA, were shifted to 1649 cm^{-1} and 1552 cm^{-1}, respectively. It was also caused by the graft copolymerization. Thus, it provided the possibility that the amphiphilic CA-*graft*-PMBMA assembled with the P(MMA-*co*-BMA) copolymers in aqueous to form core–shell structure.

As shown in Table I, the particle size of the nanoparticles, molecular weight, molar composition, and glass transition temperature of P(MMA-*co*-BMA) copolymers were investigated by DLS, GPC, ^{1}H-NMR, and DSC. The average particle size of PMBMA particles from conventional emulsion polymerization was around 80 nm with relatively broad PDI. The monodispersed PMBMA-CA nanoparticles with particle size of around 160 nm were prepared using CA instead of traditional surfactant. The number average molecular weight of P(MMA-*co*-BMA) copolymers ranged from 313,000 to 413,000 with high dispersion index. Emulsion polymerizations yielded products with high molecular weight and dispersion index[30] and the molecular weight was not affected by the macromolecular composition. This could be explained by the great radical concentration within the formed particles in respect of the rest of the mass. In the reaction system above, the composition of the monomer mixture was virtually equal to the desired copolymer composition.

Glass transition temperature (T_g) was evaluated for synthesized P(MMA-*co*-BMA) copolymers and the results are shown in Table I. For PMMA, the T_g is 118 °C while, it is 24 °C for PBMA. Introduction of BMA units within the P(MMA-*co*-BMA) copolymers increased the chain flexibility and the T_g for copolymer showed intermediate values. The PMBMA1 and PMBMA-CA1 showed T_g of 88 °C and 90 °C, respectively. Increasing the BMA segments in the copolymer, the T_g of PMBMA2 and PMBMA-CA2 were decreased to 56 °C and 52 °C, respectively. All the glass transition temperatures were consistent with the theoretical values.[25]

Transmission Electron Microscopy

TEM is an effective tool for the study of the microstructure of nanoparticles. Figure 3 displays the microstructures of PMBMA1, PMBMA-CA1 nanoparticles, NR, NR/PMBMA1, and NR/PMBMA-CA1 blending latices. PMBMA1 nanoparticles presented solids sphere [Figure 3(a)], and the particle size was estimated to be around 50–80 nm, which was consistent with the particle size analysis. As shown in Figure 3(b), monodispersed PMBMA-CA1 nanoparticles were obtained using CA instead of traditional surfactant. The PMBMA-CA1 nanoparticles showed the core–shell morphology, where P(MMA-*co*-BMA) copolymer core were coated with CA shell.[19] It could be deduced from Figure 3(b) that the particle size was around 100–120 nm, which is smaller than the results of DLS analysis. This is due to the fact that PMBMA-CA nanoparticle with hydrophilic CA shell could swell in water, leading to larger radius of the nanoparticles in water than the dried particles. For PMBMA2 and PMBMA-CA2 nanoparticles, the particle size and morphology were similar to that of PMBMA1 and PMBMA-CA1 particles [Supporting Information Figure S2(a,b)].

As seen from Figure 3(c), NR particles were spherical particles with particle size of 0.5–1 μm. The light-colored halo in their outer layer is attributed to the presence of mixed protein and phospholipids layer. After blending NR with the PMBMA1

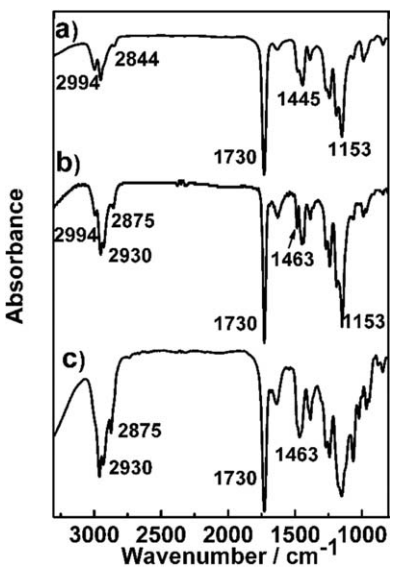

Figure 2. FTIR spectra of (a) PMMA; (b) P(MMA-*co*-BMA) copolymer from PMBMA-CA; (c) PBMA.

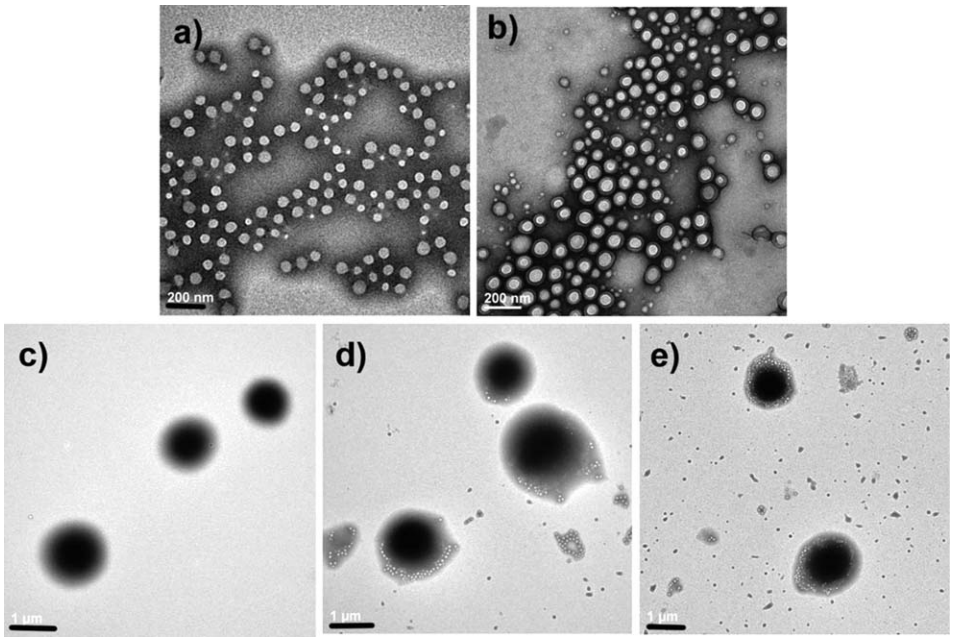

Figure 3. TEM micrographs of (a) PMBMA1; (b) PMBMA-CA1; (c) NR; (d) NR/PMBMA1; (e) NR/PMBMA-CA1; Note: the PMBMA1 and PMBMA-CA1 contents are 10%; The scale bar for (a) and (b) is 200 nm, for (c), (d) and (e) is 1 μm.

nanoparticles [Figure 3(d)], the majority of PMBMA1 nanoparticles were distributing around NR, and the rest nanoparticles aggregated together to form an external phase. For the PMBMA-CA1 nanoparticles [Figure 3(e)], several layers of PMBMA-CA1 nanoparticles were homogeneously distributed around the NR particles, and the NR particles were fully covered. The gray halo layer of NR particles almost vanished and was replaced by PMBMA-CA1 nanoparticle layers, due to the interaction of CA with the protein of NR. When the molar ratio of MMA:BMA is 5:5, the PMBMA2 nanoparticles tended to aggregate together rather than distribute around NR [Supporting Information Figure S2(c)]. It is caused by the increase of flexible aliphatic chain, which leads to self-aggregation of the nanoparticles. The microstructure of NR/PMBMA-CA2 was similar to the NR/PMBMA-CA1, as the CA shell prevented aggregation of PMBMA-CA nanoparticles.

Mechanical Properties of Modified NR Films

PMBMA and PMBMA-CA latexes with composition ratio (MMA:BMA) of 8:2 and 5:5 were prepared, and incorporated with NR via latex compounding, respectively. It is known that PMMA modified NR film has poor mechanical properties because of the incompatibility of the two phases.[13,31] However, the incorporation of soft segment PBMA into hard PMMA made the P(MMA-*co*-BMA) copolymer more flexible so that the molecular chain could easily entangle with NR. Hence, the tensile strength of PMBMA and PMBMA-CA modified NR films increased significantly compared with that of NR/PMMA film [Figure 4(a)]. The tensile strength of the modified NR film increased with increasing amount of the P(MMA-*co*-BMA) copolymers, but decreased when the content of copolymers was more than 10%. It can be explained that superfluous P(MMA-*co*-BMA) could increase the stiffness of NR film. PMBMA-CA modified NR films showed higher tensile strength than NR/PMBMA at the same composition ratio, and it could be ascribed to the better compatibility of NR/PMBMA-CA composite in the presence of CA, as the CA shell of PMBMA-CA nanoparticle [shown in Figure 3(b)] have interaction with NR.

A series of PMBMA-CA latexes with different molar composition (the ratio of MMA:BMA ranged from 10:0 to 5:5) were prepared and applied in the modification of NR. The tensile strength of NR/PMBMA-CA films were tested and presented in Figure 4(b); the weight percentage of PMBMA-CA in all NR/PMBMA-CA blend films was 10%. The PMBMA-CA nanoparticles [composition ratio (MMA:BMA) of 8:2] modified NR film showed the best tensile properties. Proper amount of PBMA in the PMBMA-CA could improve compatibility of NR and PMBMA-CA, as flexible PBMA segments could improve interfacial physical interaction of the two components. However, PBMA has inferior mechanical properties than PMMA, the reinforced performance of PMBMA-CA nanoparticles began to decrease when the composition ratio of BMA in the copolymer was over 20%. It is worthy to note that the P(MMA-*co*-BMA) nanoparticles (including PMBMA and PMBMA-CA) with a molar composition ratio of 8:2 were used for the following characterization.

Modulus could represent the relative stiffness of a material. As shown in Figure 4(c), the modulus (at 100%, 300% and 500% elongation) of NR/PMBMA1 and NR/PMBMA-CA1 films increased with increasing amount of copolymers. The behavior could be explained by the fact that the reduction of elasticity of the rubber with increase of copolymers content. This was also accompanied by a decrease in the elongation at break with increase of copolymers content [Figure 4(d)]. It could be noticed that the NR/PMBMA-CA1 films had higher modulus and lower elongation at break than that of NR/PMBMA1 films,

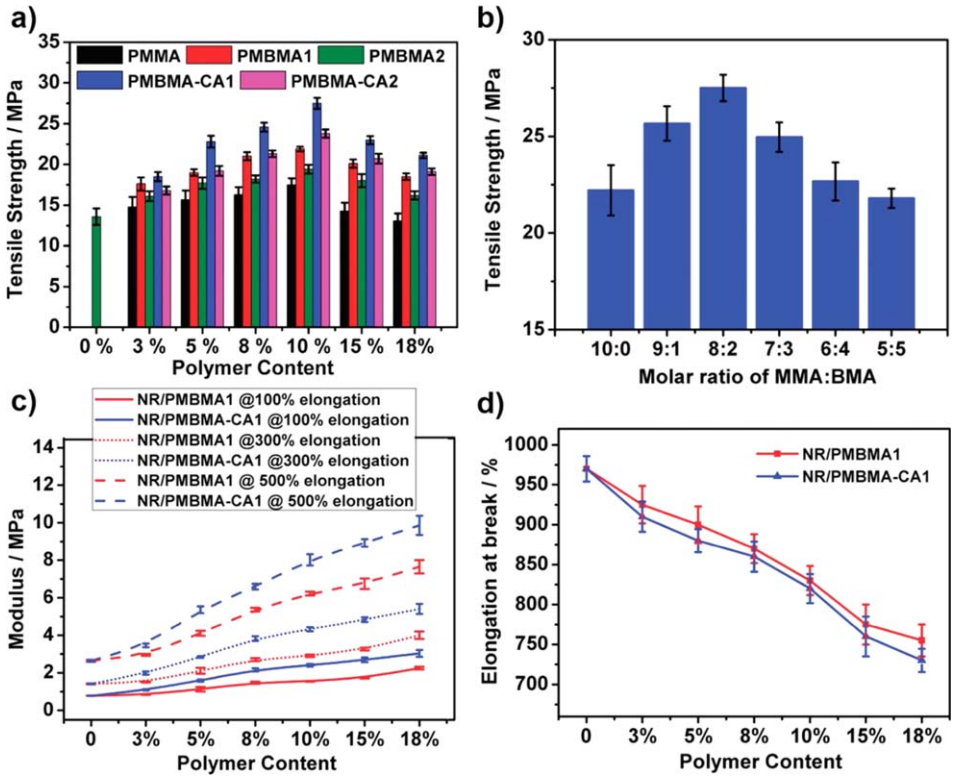

Figure 4. (a) Tensile strength of PMMA, PMBMA, and PMBMA-CA modified NR films; (b) Tensile strength of NR/PMBMA-CA films with different molar ratio (MMA:BMA); (c) Modulus of NR/PMBMA1 and NR/PMBMA-CA1 films; (d) Elongation at break of NR/PMBMA1 and NR/PMBMA-CA1 films. [Color figure can be viewed in the online issue, which is available at wileyonlinelibrary.com.]

which was attribute to stronger interaction between PMBMA-CA1 with NR in the presence of CA.

The hardness values (shore A) of neat NR, NR/PMMA, NR/PMBMA1, and NR/PMBMA-CA1 films are presented in Figure 5. The hardness of NR/PMMA film increased sharply compared with NR, as the PMMA nanoparticles tended to aggregate in the NR surface.[32] While, the hardness value of NR/PMBMA1 decreased obviously, indicating that fewer PMBMA1 nanoparticles migrated out of NR surface and thus gave better compatibility compared with PMMA and NR. The hardness of NR/PMBMA-CA1 film further decreased because of the flexible molecular chain and interaction of CA with NR, resulting in uniform distribution of PMBMA-CA1 nanoparticles in the NR matrix. The decreasing amount of PMBMA-CA1 nanoparticles on NR surface was further confirmed by SEM, atomic force microscopy (AFM), and FTIR-ATR.

Surface and Cross-Section Morphology of P(MMA-*co*-BMA) Modified NR Films

Surface morphology analysis for latex compouding films was performed by SEM and AFM, which could provide insight into the interaction between P(MMA-*co*-BMA) nanoparticles and NR.[32,33] The results are presented in Figures 6 and 7, respectively.

As seen in Figure 6(a), neat NR formed a continuous film with some holes that were mainly generated from the migration of rubber chains and water evaporation during the film formation process. When 10% of PMMA was incorporated into NR, some uneven surface with random-void morphology, caused by immiscibility of NR and PMMA particles,[15] was clearly observed [Figure 6(b)]. The latex film formation involves three stages: evaporation of water, gradual coalescence as well as deformation of soft particles, and interdiffusion of polymer chains between adjacent particles.[33,34] Upon drying, the hydrophobic and polar PMMA nanoparticles moved with the evaporating water toward the film surface. The PMMA particles were difficult to deform or diffuse into NR matrix, than aggregated on the surface. The NR/PMBMA1 film had a smoother and more flat surface compared with NR/PMMA film, and even better surface than neat NR film [Figure 6(c)]. The BMA segments have flexible

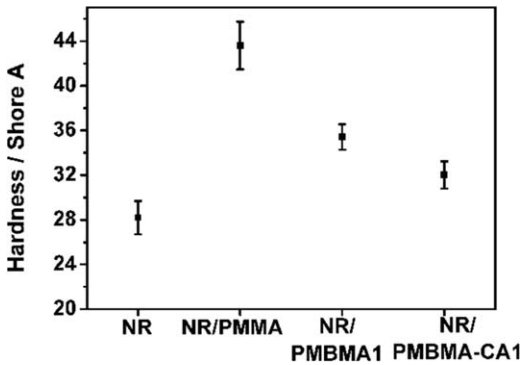

Figure 5. Hardness (Shore A) of NR, NR/PMMA, NR/PMBMA1, and NR/PMBMA-CA1. Note: the PMMA, PMBMA1, and PMBMA-CA1 contents are 10%.

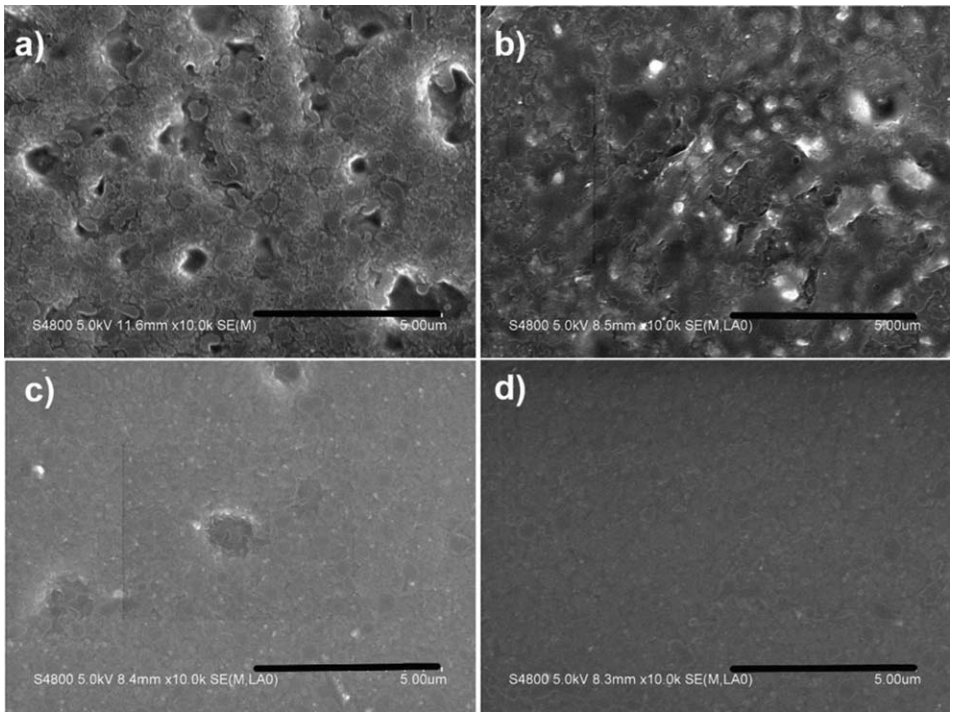

Figure 6. SEM micrographs of (a) neat NR; (b) NR/PMMA; (c) NR/PMBMA1; (d) NR/PMBMA-CA1. Note: the PMMA, PMBMA1, and PMBMA-CA1 contents are 10%, the scale bar is 5 μm.

aliphatic chains, which could benefit PMBMA1 particles to diffuse into NR matrix and improve phase adhesion in the film forming process, therefore improve the compatibility of PMBMA1 nanoparticles with NR. There were no particle aggregation and voids on the surface of NR/PMBMA-CA1 film [Figure 6(d)], indicating that the presence of CA further enhanced the interaction and compatibility of PMBMA-CA1 with NR. From TEM micrographs [Figure 3(e)], the PMBMA-CA1 nanoparticles distributed around NR particles via molecular interaction. In the process of film formation, the PMBMA-CA1 particles were fixed around NR, and embedded by soft NR molecules. In the coalescence and deformation process, PMBMA-CA1 copolymers were diffused into NR phase and thus filled the voids via the interaction; few particles migrated out of the film surface.

AFM could provide high-resolution 3D images of the film surface without disturbing the samples. The neat NR film [Figure 7(a)] showed flat surface with micro holes, which generated in the process of water evaporation. Thus, NR showed high R_a value of 142.8 nm. The NR/PMMA blend films [Figure 7(b)] exhibited much rougher surface; the R_a (229.7 nm) was much higher than that of neat NR film. The rough surface was due to the aggregation of PMMA particles on the surface as a result of incompatibility between PMMA and NR. The NR/PMBMA1 film [Figure 7(c)] showed a smooth and flat surface ($R_a = 81.6$ nm). It should be noted that the voids were much fewer and shallower in the surface of NR/PMBMA1 film compared with NR/PMMA and neat NR. In the film forming process, the flexible aliphatic chain of PMBMA1 induced the nanoparticles to penetrate into NR matrix rather than migrate out of the surface, then the microholes were filled by PMBMA1. The R_a of NR/PMBMA-CA1 film was 9.1 nm, much lower than all the films above. Figure 7(d) shows a smooth and flat surface without any voids and hills, depicting a better compatibility of PMBMA-CA1 and NR.

The cross-section morphology of the blends films were used to observe compatibility between each phase. Figure 8(a) shows the fracture surface of neat NR, which is flat and smooth. NR/PMMA film [Figure 8(b)] showed many cavities on the cross-

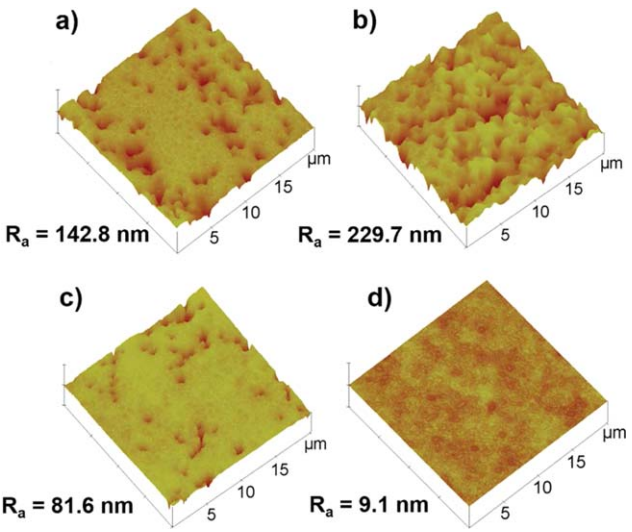

Figure 7. AFM three-dimensional images of (a) neat NR; (b) NR/PMMA; (c) NR/PMBMA1; (d) NR/PMBMA-CA1. Note: the PMMA, PMBMA1, and PMBMA-CA1 contents are 10%. [Color figure can be viewed in the online issue, which is available at wileyonlinelibrary.com.]

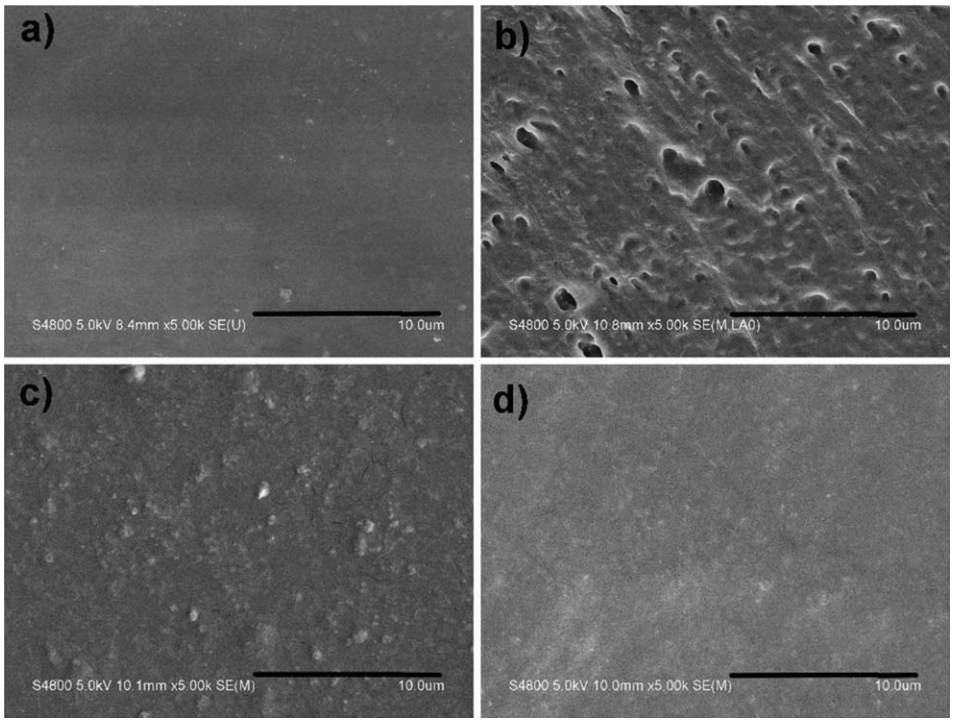

Figure 8. Cross-section micrographs of (a) neat NR; (b) NR/PMMA; (c) NR/PMBMA1; (d) NR/PMBMA-CA1. Note: the PMMA, PMBMA1, and PMBMA-CA1 contents are 10%, the scale bar is 10 μm.

section, indicating that NR and PMMA are incompatible. The morphology of NR/PMBMA1 [Figure 8(c)] presented no cavities, which was attributed to improved compatibility between NR and PMBMA1 in the presence of flexible butyl chain. The particle aggregations in cross-section of NR/PMBMA1 were caused by hydrophobic interaction between PMBMA1 nanoparticles. NR/PMBMA-CA1 [Figure 8(d)] shows a fine and uniform phase. This means that there is an effective interfacial interaction in the blends leading to better compatibility.

Fourier Transform Infrared-Attenuated Total Reflection (FTIR-ATR)

The FTIR-ATR spectra of the film surface of various latex compounding films, including neat NR and NR/PMMA film as controls, are given in Figure 9. The spectroscopy of neat NR [Figure 9(a)] was characterized by the absorbance peaks at 1660 cm^{-1}, 1445 cm^{-1}, 1375 cm^{-1}, and 836 cm^{-1}, which were attributed to C═C stretching, C—H bending of CH_2, C—H bending of CH_3, and C═CH wagging, respectively. In addition, the small peak at 1554 cm^{-1} was assigned as the N—H bending of the protein,[26] which indicated the protein layer existed in NR latex. While, PMMA and P(MMA-*co*-BMA) copolymers had characteristic absorption peaks at 1730 cm^{-1} and 1148 cm^{-1}, that corresponded to C═O stretching and C—O stretching vibration. The spectrum of NR/PMMA film [Figure 9(b)] revealed a strong absorbance peak at 1730 cm^{-1} and 1148 cm^{-1} associated with the characteristic peaks of NR. This clearly demonstrated the preferential enrichment of PMMA particles at the surface of NR film, as the FTIR-ATR spectroscopy measures the surface characteristic to several microns deep. For the NR/PMBMA1 film [Figure 9(c)], the intensities of C═O and C—O characteristic peaks at 1730 cm^{-1} and 1148 cm^{-1} decreased with same addition of copolymers (10% of NR), meaning that the PMBMA1 particles were reduced on the surface of NR. NR/PMBMA-CA1 [Figure 9(d)] had the weakest peak of C═O, and the peak at 1148 cm^{-1} disappeared, indicating that only small amount of PMBMA-CA1 particles migrated out of the surface in the process of film formation. Also, the characteristic peak of N—H shifted to 1563 cm^{-1}, showing that there was interaction between NR and PMBMA-CA1. The FTIR-ATR results are consist with SEM and AFM analyses, suggesting that the PMBMA-CA1 had the best compatibility with NR, therefore, less PMBMA-CA1 nanoparticles migrated out of NR surface.

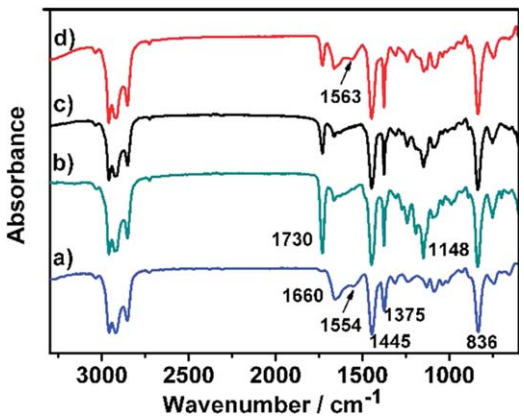

Figure 9. The FTIR-ATR spectra of (a) neat NR; (b) NR/PMMA; (c) NR/PMBMA1; (d) NR/PMBMA-CA1. Note: the PMMA, PMBMA1, and PMBMA-CA1 contents are 10%. [Color figure can be viewed in the online issue, which is available at wileyonlinelibrary.com.]

DSC Characterization

To further confirm the compatibility between NR and P(MMA-*co*-BMA) copolymer, DSC was used to analyze the glass transition temperatures of the modified NR films (Supporting Information Figure S3). The T_g of neat NR was −65.33 °C. Moreover, the T_g of NR/PMBMA1 and NR/PMBMA-CA1 blended films shifted to −61.54 °C and −61.18 °C, respectively. The results indicated that some interactions between the P(MMA-*co*-BMA) nanoparticles and NR led to the formation of the miscible polymer networks, which can be considered as an improvement in interfacial adhesion between the blend components. Furthermore, no disguised signal was observed in the DSC thermograms, which also indicated that all the ingredients in the blended film were compatible.[35]

CONCLUSIONS

In this study, a series of P(MMA-*co*-BMA) nanoparticles were synthesized via emulsion polymerization using traditional emulsifier or CA. Monodispersed, core–shell PMBMA-CA nanoparticles were produced when using CA as surfactant. The synthesized PMBMA and PMBMA-CA latexes were incorporated into NR via latex compounding. The microstructure of PMBMA1, PMBMA-CA1 nanoparticles, and modified NR latexes was investigated by TEM, from which the core–shell structure of PMBMA-CA was observed and the nanoparticles distributed around NR. For the NR/PMBMA-CA1, the gray halo layer of NR particles virtually disappeared and was replaced by PMBMA-CA1 nanoparticle layers, meaning that the PMBMA-CA1 particles immerged into the outer layer via the interaction of CA and NR. The mechanical properties of modified NR films with different composition ratios and copolymer content were studied. NR/PMBMA-CA1, with a molar composition ratio (MMA:BMA) of 8:2, showed maximum tensile strength, where the addition of copolymer was 10%. The outstanding mechanical properties of NR/PMBMA-CA1 film were caused by the better compatibility in the presence of CA and soft segments BMA. From the SEM and AFM results, NR/PMBMA-CA1 film presented a smooth surface with low roughness value, indicating that the interaction of CA and proteins of NR could prevent PMBMA-CA1 nanoparticles from migrating out of the film surface. FTIR-ATR spectra confirmed that fewer PMBMA-CA1 particles migrated out of film surface, and interaction existed between PMBMA-CA1 and NR. Furthermore, the increasing T_g values of PMBMA1 and PMBMA-CA1 modified NR films further proved the compatibility between the two phases. It was thus demonstrated that PMBMA-CA1 is more compatible with NR than PMMA and PMBMA1, and the composite films make the copolymers high interest for the preparation of dipped products with excellent tensile strength and elasticity.

ACKNOWLEDGMENTS

This work was supported by Fundamental Research Funds for the Central Universities (22A201514002).

REFERENCES

1. Rajan, V. V.; Dierkes, W. K.; Joseph, R.; Noordermeer, J. W. M. *Prog. Polym. Sci.* **2006**, *31*, 811.
2. Ho, C. C.; Kondo, T.; Muramatsu, N.; Ohahima, H. *J. Colloid Interface Sci.* **1996**, *178*, 442.
3. Nawamawat, K.; Sakdapipanich, J. T.; Ho, C. C.; Ma, Y.; Song, J.; Vancso, J. G. *Colloid Surf. A* **2011**, *390*, 157.
4. Ho, C. C.; Khew, M. C. *Langmuir* **1999**, *15*, 6208.
5. Wu, L.; Qu, P.; Zhou, R.; Wang, B.; Liao, S. *High Perform. Polym.* **2014**, *27*, 486.
6. Piya-areetham, P.; Rempel, G. L.; Prasassarakich, P. *Polym. Degrad. Stabil.* **2014**, *102*, 112.
7. Jayasuriya, M. M.; Hourston, D. J. *J. Appl. Polym. Sci.* **2009**, *112*, 3217.
8. Ochigbo, S. S.; Luyt, A. S.; Focke, W. W. *J. Mater. Sci.* **2009**, *44*, 3248.
9. Chuayjuljit, S.; Moolsin, S.; Potiyaraj, P. *J. Appl. Polym. Sci.* **2005**, *95*, 826.
10. Asaletha, R.; Bindu, P.; Aravind, I.; Meera, A. P.; Valsaraj, S. V.; Yang, W.; Thomas, S. *J. Appl. Polym. Sci.* **2008**, *108*, 904.
11. Cheo, S. H. Y.; Wang, P.; Tan, K. L.; Ho, C. C.; Kang, E. T. *J. Mater. Sci. Mater. Med.* **2001**, *12*, 377.
12. Oommen, Z.; Thomas, S. *Polym. Bull.* **1993**, *31*, 623.
13. Oommen, Z.; Nair, M. R. G.; Thomas, S. *Polym. Eng. Sci.* **1996**, *36*, 151.
14. Oommen, Z.; Thomas, S. *J. Mater. Sci.* **1997**, *32*, 6085.
15. Thiraphattaraphun, L.; Kiatkamjornwong, S.; Prasassarakich, P.; Damronglerd, S. *J. Appl. Polym. Sci.* **2001**, *81*, 428.
16. Nakason, C.; Panklieng, Y.; Kaesaman, A. *J. Appl. Polym. Sci.* **2003**, *92*, 3561.
17. Nakason, C.; Saiwaree, S.; Tatun, S.; Kaesaman, A. *Polym. Test.* **2006**, *25*, 656.
18. Sanguansap, K.; Thonggoom, R.; Tangboriboonrat, P. *Eur. Polym. J.* **2006**, *42*, 2334.
19. Zhu, J.; Li, P. *J. Polym. Sci. Part A: Polym. Chem.* **2003**, *41*, 3346.
20. Mao, X.; Huang, J.; Leung, M. F.; Du, Z.; Ma, L.; Huang, Z.; Li, P.; Gu, L. *Appl. Biochem. Biotechnol.* **2006**, *135*, 229.
21. Li, P.; Zhu, J.; Sunintaboon, P.; Harris, F. W. *Langmuir* **2002**, *18*, 8641.
22. Varkey, J. T.; Thomas, S.; Rao, S. S. *J. Appl. Polym. Sci.* **1995**, *56*, 451.
23. Varkey, J.; Augustine, S.; Groeninickx, G.; Bhagawan, S. S.; Rao, S. S.; Thomass, S. *J. Polym. Sci. Part B: Polym. Phys.* **2000**, *38*, 2189.
24. Sarac, A. S. *Prog. Polym. Sci.* **1999**, *24*, 1149.
25. Silvestri, D.; Gagliardi, M.; Cristallini, C.; Barbani, N.; Giusti, P. *Polym. Bull.* **2009**, *63*, 423.
26. Pichayakorn, W.; Suksaeree, J.; Boonme, P.; Taweepreda, W.; Ritthidej, G. C. *Ind. Eng. Chem. Res.* **2012**, *51*, 13393.
27. Vail, N. K.; Barlow, J. W.; Beaman, J. J.; Marcus, H. L.; Bourell, D. L. *J. Appl. Polym. Sci.* **1994**, *52*, 789.
28. Souza, N. L. G. D.; Brandão, H. M.; de Oliveira, L. F. C. *Polym. Plast. Technol.* **2014**, *53*, 319.

29. Ávila-Ortega, A.; Aguilar-Vega, M.; Loría Bastarrachea, M. I.; Carrera-Figueiras, C.; Campos-Covarrubias, M. *J. Polym. Res.* **2015**, *22*, 226.

30. Gaboyard, M.; Jeanmaire, T.; Pichot, C.; Hervaud, Y.; Boutevin, B. *J. Polym. Sci. Part A: Polym. Chem.* **2003**, *41*, 2469.

31. Nakason, C.; Pechurai, W.; Sahakaro, K.; Kaesaman, A. *J. Appl. Polym. Sci.* **2006**, *99*, 1600.

32. Ho, C. C.; Khew, M. C.; Liew, Y. F. *Surf. Interface Anal.* **2001**, *32*, 133.

33. Feng, J.; Winnik, M. A.; Shivers, R. R.; Clubb, B. *Macromolecules* **1995**, *28*, 7671.

34. Ho, C. C.; Khew, M. C. *Langmuir* **2000**, *16*, 2436.

35. Pichayakorn, W.; Suksaeree, J.; Boonme, P.; Amnuaikit, T.; Taweepreda, W.; Ritthidej, G. C. *J. Membr. Sci.* **2012**, *411–412*, 81.